applied sciences

MDPI

Article

Numerical Investigation of Thermal Efficiency of a Solar Cell

Emaad Ansari [1], Mohammad Nishat Akhtar [1], Wan Amir Fuad Wajdi Othman [2,*], Elmi Abu Bakar [1,*] and S. S. N. Alhady [2]

[1] School of Aerospace Engineering, Universiti Sains Malaysia, Nibong Tebal 14300, Penang, Malaysia
[2] School of Electrical and Electronic Engineering, Universiti Sains Malaysia, Nibong Tebal 14300, Penang, Malaysia
* Correspondence: wafw_othman@usm.my (W.A.F.W.O.); meelmi@usm.my (E.A.B.); Tel.: +60-19-6691441 (W.A.F.W.O.); +60-16-4939839 (E.A.B.)

Abstract: Solar air and water heaters are beneficial in many countries across the globe where solar radiation is massive in the daytime. As the surface temperature of the photovoltaic cell increases, the efficiency of the cell scales down. We carried out the cooling of solar panels in order to maximize their efficiency. In the present work, we examined the dependence of the inlet boundary condition on the area average temperature at the outlet of the tube. The tube comprises a square cross-section and carries three folds in order to maximize the area in contact with a solar panel. We investigated the dependency of thermal efficiency of solar panels on inlet boundary conditions and observed that with the increase in Reynolds number, i.e., velocity at the inlet, the thermal efficiency initially increases up to $Re = 700$ and then remains constant at 94%. We also found that when 40% of the heat input was carried away by cooling water, 20% electrical efficiency was achieved.

Keywords: numerical investigation; thermal efficiency; solar cell; computational fluid dynamics (CFD) applications; mesh-based numerical methods

check for updates

Citation: Ansari, E.; Akhtar, M.N.; Othman, W.A.F.W.; Abu Bakar, E.; Alhady, S.S.N. Numerical Investigation of Thermal Efficiency of a Solar Cell. *Appl. Sci.* **2022**, *12*, 10887. https://doi.org/10.3390/app122110887

Academic Editor: Stefan Bordihn

Received: 16 September 2022
Accepted: 19 October 2022
Published: 27 October 2022

Publisher's Note: MDPI stays neutral with regard to jurisdictional claims in published maps and institutional affiliations.

Copyright: © 2022 by the authors. Licensee MDPI, Basel, Switzerland. This article is an open access article distributed under the terms and conditions of the Creative Commons Attribution (CC BY) license (https://creativecommons.org/licenses/by/4.0/).

1. Introduction

The burning of fossil fuels has degraded the quality of the environment to a great extent. The need for production of cleaner energy to save the environment has led researchers to increase the efficiency of non-conventional methods of energy production, as their efficiencies are quite low. Because of the rapid growth in a share of non-conventional electrical energy production, there is a need for efficient technology to ensure the operation of renewable energy sources at the highest possible efficiency. Since the photovoltaic (PV) costs per 1 kW are decreasing every year, the PVs attract attention of the potential end users. However, the nominal efficiency of PV panels is low (maximum 26.7% for monocrystalline laboratory set and maximum 24.4% for multi-crystalline silicon wafers) [1] and it is decreasing (0.5% per 1 °C if temperature is higher than 25 °C) with the PV surface temperature. Therefore, even during a day with high solar irradiation, the electrical energy production from PV is lower than expected. Therefore, to maintain the high electrical energy conversion efficiency, there is a need to propose an efficient method for the cooling of PV panels. Multiple studies had been carried out in the past, suggesting various techniques for improving PV cell efficiencies. We carried out a brief review of the existing literature.

Sharaf et al. [2] noted that a part of the incoming sunlight converts to energy on the solar cell's surface, whereas the remaining sunlight absorbs within the cell. As a result, its surface temperature increases. The greater the surface temperature, the worse the transformation efficiency (the proportion of solar energy received by a PV device that is transformed into useful power), and the weaker the long-term durability. Verma et al. [3] observed that the solar cells have a low electrical efficiency (in most cases around 12–15%). Although sunshine was necessary for generating power, the rate of warming at the underside of the cell had a negative impact on the efficiency. They related the increase in

temperature to the conversion of sunlight's energy into heat, and it may have a detrimental impact on the electrical parameters and the cell's life span. Using cooling measures would reduce the amount of heat generated and lower the overall temperature of the cell. We can cool solar cells using a variety of approaches, including forced air/water flow, hybrid PV/thermal systems, and phase change material-based PV applications [4]. According to the results of some studies on passive and active cooling strategies, Ghadikolaei [5] concluded that the flow rate in the water cooling method had a direct relationship with the reduction in temperature and rise in cell efficiency. We mention the effect of cooling techniques on the cell efficiencies in the literature highlighting the benefits of cooling PV modules.

Akbarzadeh and Wadowski [6] used a unique reflector for this purpose and installed a heat pipe for the cooling of PV modules to maximize the power output. Anderson et al. [7] used a heat pipe for cooling the concentration PV (CPV) module. They used a natural convection through a heat pipe with aluminum fins that rejected a heat flux of 40 W/cm^2 to the atmosphere. This helped in maintaining the rise in cell temperature by only 40 °C compared with the ambient temperature. Abdolzadeh and Ameri [8] sprayed water on the front surface of the PV cell to improve the effectiveness of the water pumping system. The results proved that spraying water could enhance PV cell efficiency by 3.26% and total system efficiency by 1.35% at 16 m pumping head. Azadeh [9] used a thin film of water on the PV array to cool the surface and increase electrical efficiency. He reported two vital parameters of this method, i.e., array of nominal power and system head, and concluded that a decrease in nominal power and increase in system head generates more power. Abdul Hai [10] proposed a method to reduce cell temperature by installing a clay at the back of the module and evaporating water. The results of his experiment showed that he achieved a 19.4% maximum increase of output voltage and 19.1% better output power by incorporating this method. Brinkworth et al. [11] carried out a simulation to show that cladding below the PV cell can increase the efficiency of the PV module significantly. PV modules installed on roofs may not be efficient because of high temperatures. Therefore, they installed an air duct behind the PV arrays, which reduced the temperature by 15–20 K, which increased the electrical output of the system. Bione et al. [12] compared the performance of PV pumping systems using various generators. They used fixed, tracking, and V-trough generators in the experiments. The primary aim of the experiment was to reduce the cost incurred in pumping, and they found out that a tracking system reduces cost by 19% whereas the concentration system reduced cost by 48%. Bahaidarah et al. [13] focused on thermal and electrical performance and concluded that continuous cooling of the module enhances thermal efficiency by 9% to 20%. The water-cooling system produces 750 W relative to 190 W, which was produced by a simple PV system at an irradiance level of 900 W/m^2.

Chen et al. [14] inspected whether the saturated moist air used in evaporative cooling would enhance the efficiency of the cooling system. Du et al. [15] discovered that a water-cooled CPV module produces 4.7 to 5.2 times more electricity than a normal PV cell does. A magnitude of 71.13 W of electrical power was produced, contrary to a magnitude of 16.55 W produced by a fixed one. Farahat [16] used a water cooling technique and a heat pipe to reduce the operating temperature of PV arrays for maximum electrical energy and efficiency of the system. Hughes et al. [17] performed a CFD analysis and incorporated a heat pipe behind PV cells to reduce the working temperature of PV cells. The heat pipe reduces the temperature up to 30 °C, thus increasing the power output and hence the efficiency of the PV panel. Hasan et al. [18] reported the cooling of a PV cell using micro-jets of water from the front face with variation in Reynolds number (*Re*) ranging from 10,000 to 30,000. Irwan et al. [19] conducted an indoor test to study the behavior of water-cooled PV cells for incident solar radiations of 413, 620, 821, and 1016 W/m^2. A drop in the temperature of 5–23 °C of the PV cell was observed with the help of cooling water, which leads to the increase in thermal efficiency by 9–22%. Kerzmann and Schaefer [20] numerically analyzed a linear concentrating PV cell (LCPV) cooled using a fluid. Kok and Woei [21] proposed an automobile radiator geometry for the cooling of a PV cell. The cooling of the CPV module

improves conversion efficiency from 22.39% to 26.85%. Furthermore, the radiator helps in cooling the temperature from 59.4 °C to 32.1 °C.

Masayuki et al. [22] observed that a water-cooled solar array was about 3% more useful than a normal one. Nizetic et al. [23] studied the effect of water impingement on the PV cell and observed a 16.3% increase in thermal efficiency. Additionally, the maximum electrical efficiency enhancement of 14.1% was achieved by water cooling with peak solar irradiance. The cooling technique reduces the temperature of the panel from 54 °C (without water cooling) to 24 °C, with cooling from both sides of the PV panel. Omubo et al. [24] found that the maximum power of 16 W was achieved at 43 °C. Park et al. [25] found that a 1 °C increase in temperature decreases power by 0.52% in outdoor conditions when irradiation was 500 W/m^2. Royne et al. [26] focused on cooling PV cells under concentrated illumination. An active cooling having a thermal resistance of less than 10^{-4} m^2K/W is necessary for the proper functioning of densely packed solar PV cells (>150 suns). It was proved that such a low thermal resistance is possible only by using micro-channels and impinging jets. Stefan [27] found that with per unit temperature increase in PV cells, the temperature of water decreases by 0.4%. Using the water flow over the front surface of the PV cells, the temperature of the cell drops up to 22 °C. This magnitude of temperature drops yields a 10.3% rise in electrical power output. Saad and Masud [28] reported cooling of the PV array by circulating water from the front surface and studied its efficiency. It was concluded that up to 15% increase in efficiency could be achieved at peak irradiations using this technique. Furthermore, a vast amount of heat loss (50%) was observed due to the direct contact of PV cells with water. It was also found that water cooling keeps the module free from dust and dirt particles. This leads to some increase in electrical efficiency. Skoplaki and Palyvos [29] found out various correlations to understand the dependency of the electrical performance of PV cells on operating temperature. It was concluded that output voltage and efficiency both are indirectly proportional to the operating temperature and they decrease with an increase in the temperature in all conditions. Shafiqur and Rehman [30] analyzed the performance of 5.28 kW capacity PV cells installed at KFUPM, Saudi Arabia. It was clearly visible that energy yield was highest at 35.8 °C and it decreased with an increase in temperature. Salih et al. [31] used the water spray impingement technique to enhance the performance of PV arrays. Because of the cooling of modules, an enhancement of 12% in the electric power output was observed. Overall, a gain of 215 W in output power was reported because of cooling. Additionally, the temperature decrease from 60.5 °C to 28.5 °C in 5 min was observed due to water impingement. Teo et al. [32] performed experiments on a PV cell, with and without air cooling, and found a linear relationship between the temperature of modules and its efficiency. Without cooling the PV cells, only 8–9% of conversion efficiency was possible. However, with active cooling, the temperature decreased gradually, and a 12–14% enhancement in conversion efficiency was observed. Furthermore, using an air blower to cool down the PV cells reduced the temperature of the cell significantly.

The validation of the numerical model of the PV panels cooling system with an experimental setup was carried out in the present study. Experiments were carried out for determining the thermal efficiency by measuring the temperature at the outlet. This was done at two mass flow rates (0.025 kg/s and 0.5 kg/s). Energy balance was conducted for the heat losses in order to calibrate the setup. The validation of the computational domain was successfully managed by specifying the boundary conditions. Simulations were carried out at different values of the velocity inlet in order to develop a correlation between the Re at the inlet and the thermal efficiency. The correlations were developed as semi-empirical relations. Last, the semi-empirical relation developed was validated with other literature work.

2. Materials and Methods

2.1. Experimental Setup

2.1.1. Description of the Experimental Setup

An experimental setup was designed and fabricated at 18.7518° N, 73.5514° E and positioned at the roof to investigate the effect of water-based cooling on the voltage-current (VI) characteristics of the PV collector (Figure 1). Abundant availability and many applications of water attracted attention as a heat transfer medium. Anodized aluminum of 3 mm thickness and 82% reflectivity was used for the fabrication of the heat exchanger. The heat exchanger of square cross section was preferred because of high thermal conductivity, better surface contact, and its light weight.

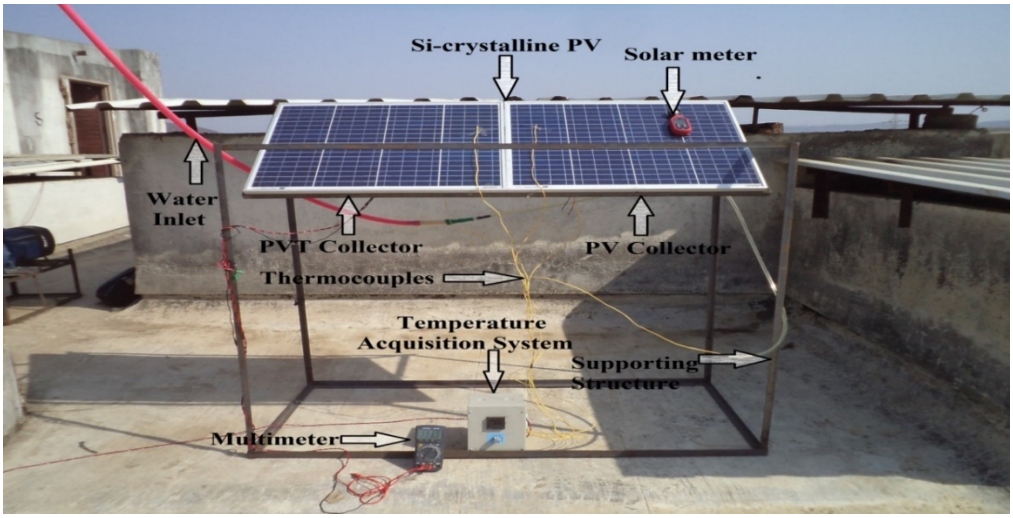

Figure 1. Experimental setup.

The rectangular flow design improved surface contact time with PV that can be supportive of extracting maximum heat from the PV module. A commercial Si-based multi-crystalline PV module of 50 W capacity and 0.55 m × 0.65 m size was under investigation, and the heat exchanger was attached at the back of the PV module. The insulation was provided from the backside to avoid thermal loss by convection. Water flows from the tank through the pipe, and the flow rate was measured by an acrylic rotameter (±3%). The water passed through a heat exchanger and extracts heat of the PV module (Figure 2).

K-type thermocouples with an accuracy of 0.7 °C were placed at various locations, such as the tank, the inlet to the heat exchanger, the outlet of the heat exchanger, and the surface of the PV module, and were connected to the temperature acquisition system. The VI characteristics of the PV module are recorded with a digital multi-meter. The MECO-made digital solar meter (±10 W/m^2) was used to measure solar irradiance falling on the PV module. PV modules with supporting instruments were fixed on the supporting stand at a height in the east-west direction to face the sun with no obstruction. The wind speed over the collector was measured with a vane-type anemometer PCE-VA 11 with ±3% uncertainty.

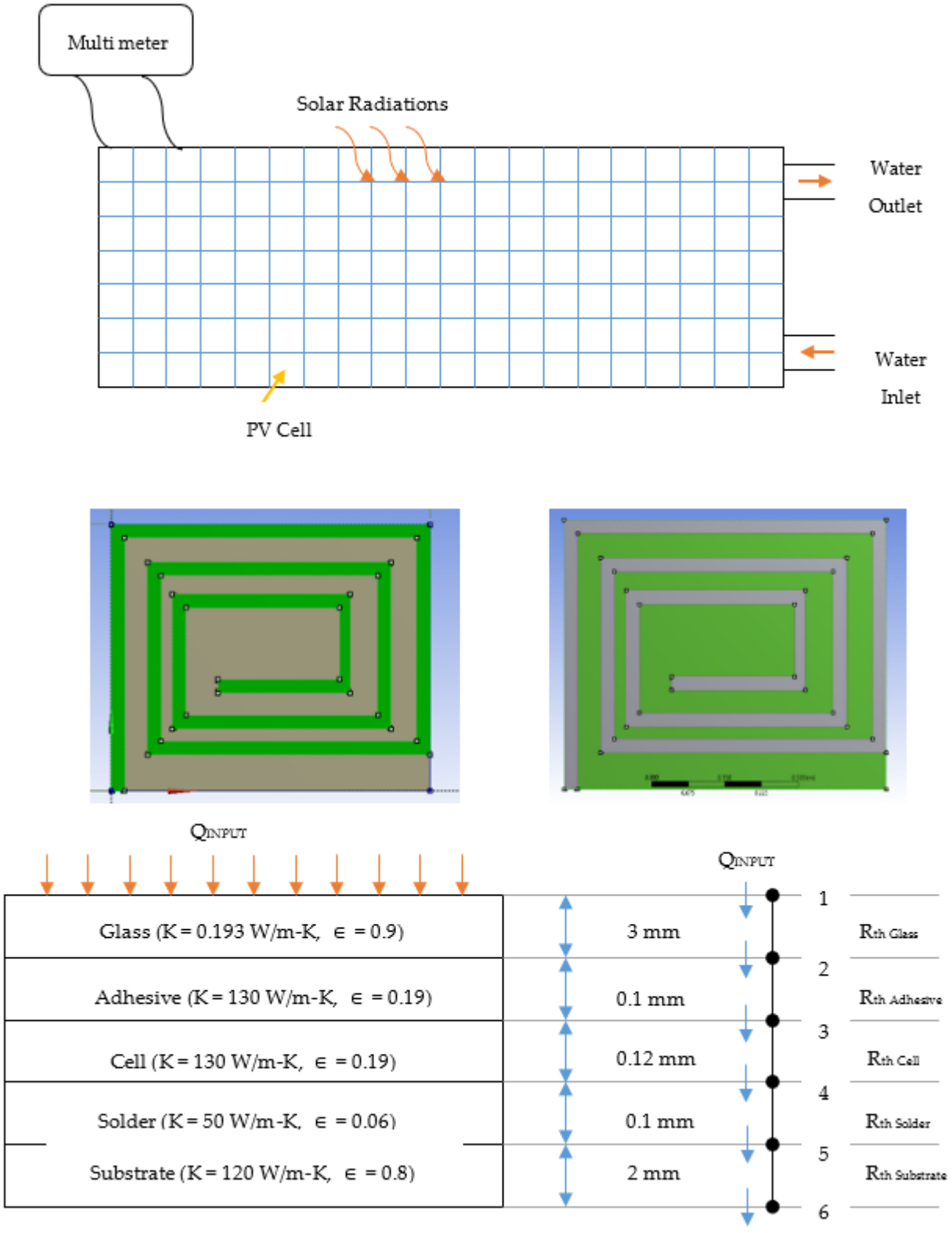

Figure 2. Top view of PV panel, back view of PV panel, and thermal resistance for individual component of PV cells.

2.1.2. Heat Balance of the Experimental Setup

In order to balance the heat input against the heat lost, and the heat gained by the water, uncertain heat transfer was calculated for different values of net heat input. Net

heat input is the total solar radiation incident minus the electrical power output, as shown in Equation (1), which was further used to calculate the absorbed heat (Equation (2)). The electrical power output is measured with the help of a digital multi-meter (Figure 2). Experiments were carried out for various heat inputs to the PV cell ranging from 2 W to 30 W and the mass flow rate of water being fixed to 0.025 kg/s. Heat loss because of conduction and radiation from the cross-section surface of PV cells were individually accounted for every material (Figure 2) using the commercial equation of conduction and radiation Equations (4) and (5). The average temperature in line with the thickness of the PV cell at the individual surface was calculated using Equation (3).

$$Q_{net,\,input} = Q_{input} - Q_{Electrical} \tag{1}$$

$$Q_{absorbed} = 0.93 \times Q_{net,\ input} \tag{2}$$

$$T_j = T_i - \frac{L_{ij}}{K_{mat} A_{s\ mat}} \times Q_{\ absorbed} \tag{3}$$

$$Q_{Cond} = K_{Mat} \times A_{s\ Mat} \times \left(\frac{T_j + T_i}{2} - T_a \right) \tag{4}$$

$$Q_{Rad} = \sigma \varepsilon A_{s\ Mat} \times \left[\left(\frac{T_i + T_j}{2} \right)^4 - {T_a}^4 \right] \tag{5}$$

$$Q_{Conv,\ \ PV\ Cell\ Bottom} = h_{c,\ Air} \times A_{PV\ cell} \times (T_6 - T_a) \tag{6}$$

$$Q_{Rad,\ PV\ Cell\ Bottom} = \sigma \varepsilon A_{PV\ cell} \times \left({T_6}^4 - {T_a}^4 \right) \tag{7}$$

$$Q_{water} = m' \times C_{p,water} \times (T_{water,\,out} - T_{water,\,in}) \tag{8}$$

The convection and radiation heat loss from the back surface of the PV cell was accounted for by using Equations (6) and (7) (Figure 2). A similar method was adopted for calculating the heat transfer because of convection and radiation from the pipe surface exposed to the atmosphere (Figure 2). Figure 3 shows the actual surface responsible for heat transfer because of convection and radiation from the pipe surface. Last, the temperature difference between the inlet and outlet of the heat exchanger was measured, which enables the magnitude of heat gained by the water (Equation (8)). The heat transfer through physical modes of heat transfer highly depended on human skills, thus increasing the probability of calculation errors in model validation.

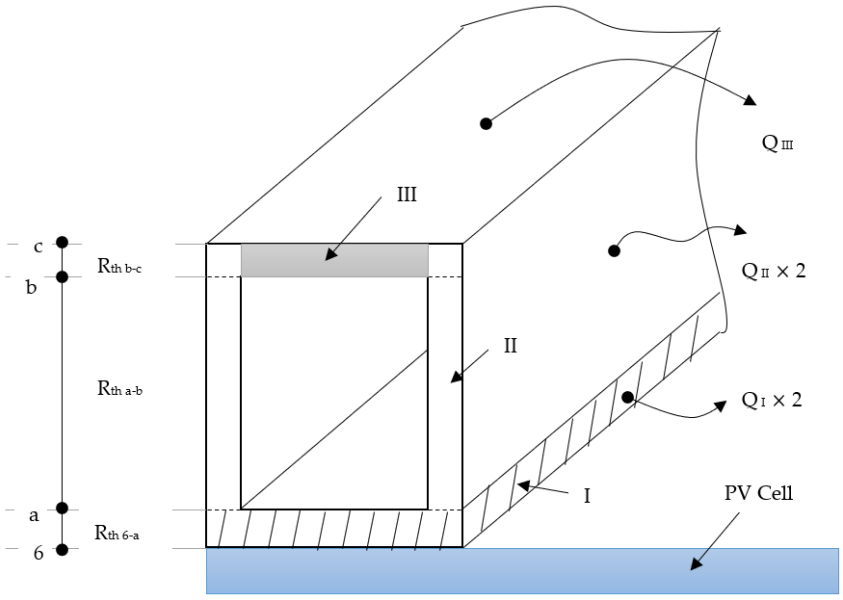

Figure 3. Components of heat lost from various surfaces of the pipe.

In order to validate the results of thermal efficiency computed numerically, a graph of theoretical efficiency versus numerical efficiency is plotted later in the Results and Discussion section. The numerical efficiency was calculated using numerically computed temperature of water at the outlet, while the theoretical efficiency is defined using Equation (9). In Equation (9), the suffix T and N stand for theoretical and numerical, respectively.

$$\eta_{thermal\ T,\ N} = \frac{m' \times C_{p,water} \times (T_{water,\ out} - T_{water,\ in})}{Q_{net,\ input}} \quad (9)$$

2.2. Numerical Setup

2.2.1. Grid Independence Test

In order to study the variation in results because of grid size, several elements throughout the computational domain are varied from 400,000 to 1,300,000. Boundary conditions in all the cases were fixed. The simulation was carried out at a heat input of 326 W/m^2 with a water inlet mass flow rate of 0.025 kg/s. The minimum and maximum face size used in performing grid independence tests were 3.25×10^{-4} and 3.25×10^{-3} (Figure 4); only the number of elements in the computational domain was varied. A commercial tetrahedral mesh is used in a basic solver pack of ANSYS CFX 18.3, ANSYS Inc., Canonsburg, PA, USA.

As seen in Figure 5, implementing several elements above 1,263,000 shows the same temperature across the outlet. Hence, the use of grid size carrying 1,263,000 number of nodes is optimal for achieving accurate results. The computational time required for convergence using this grid size is 3 h with 12 core of the processor on the server.

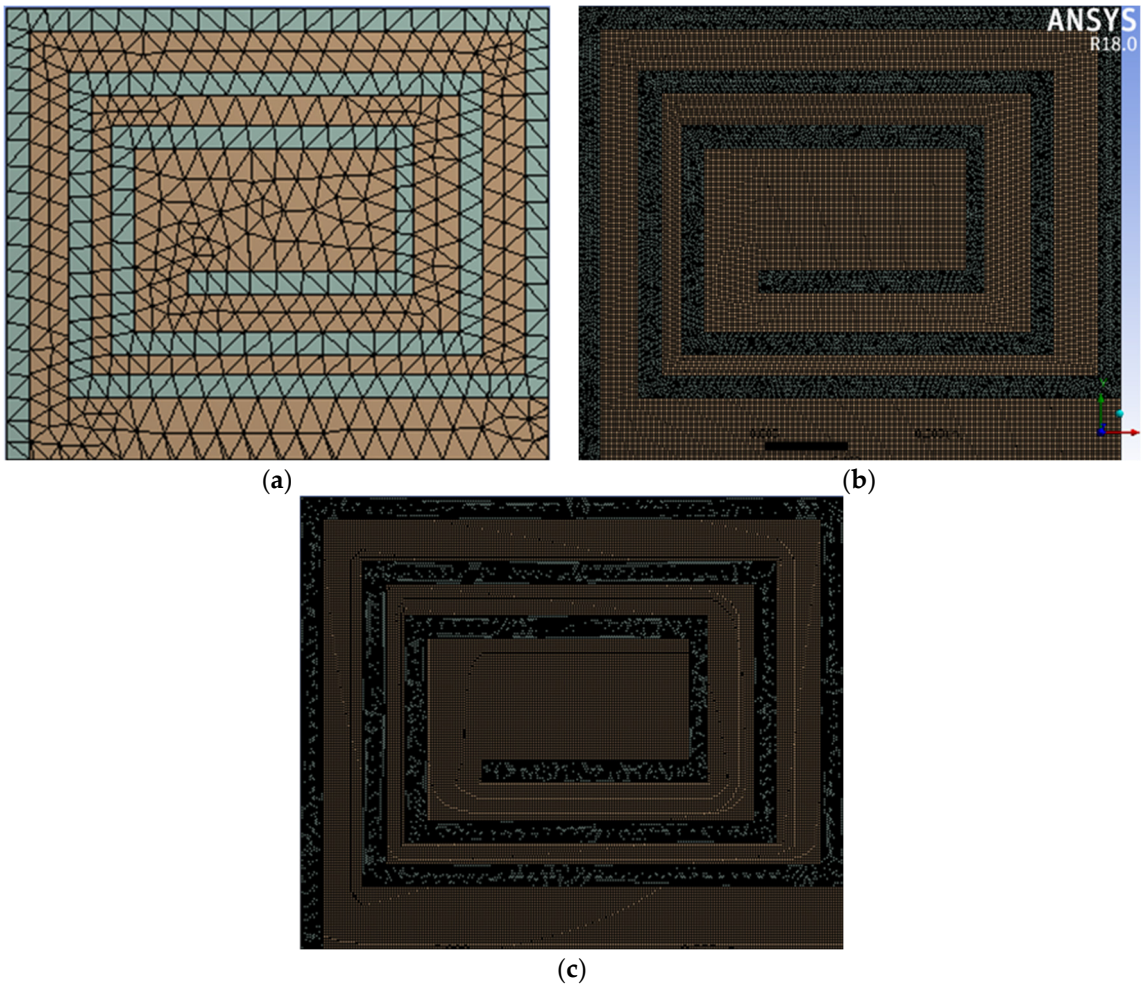

Figure 4. Computational grid: minimum face size = 3.25×10^{-4}, maximum face size = 3.25×10^{-3}. (**a**) Number of elements 12,000; (**b**) number of elements 1,000,000; (**c**) number of elements 1,263,000.

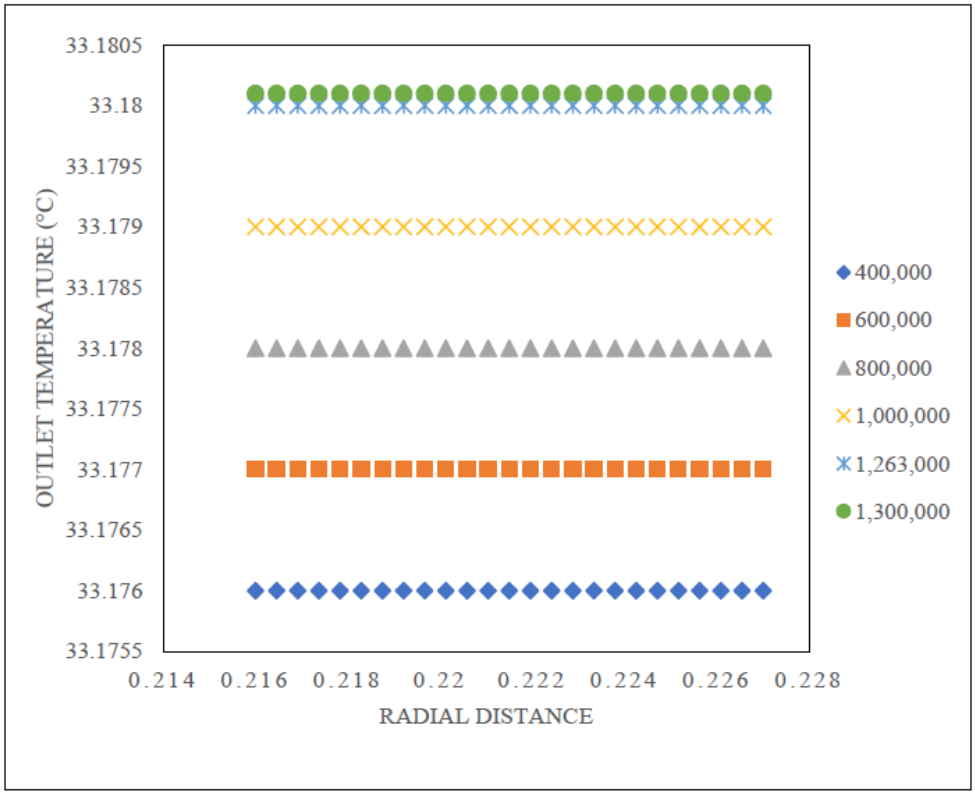

Figure 5. Outlet temperature for various number of elements ranging from 400,000 to 1,300,000.

2.2.2. Turbulence Models and Computation Specifications

For the variation of *Re* in the laminar region, a k-Epsilon turbulence model was used to predict the flow profile; whereas for the turbulent flow, an SST turbulence model was used for predicting the flow (Appendix A). Figure 6 shows that the k-Epsilon model shows the most accurate results as compared with the experimental ones. Additionally, k-Epsilon is the only model which incorporates laminar flow in the CFX solver. Hence, the k-Epsilon model was used since water flow was laminar. The simulation was carried in commercial ANSYS CFX pack (Version 18.3).

To incorporate the heat transfer effect, a basic thermal model in the solver setting was kept on. The Monte Carlo radiation method was incorporated to consider the radiation heat lost with the Gray point of 1000. The turbulent intensity at the inlet was kept constant at 9%, as no effect is observed with variation in turbulent intensity. High-resolution solver setting was adopted instead of first order with double precision for the most accurate prediction of the temperature profile at the outlet. Not much effect of wind speed on the thermal efficiency was observed. However, 15 knots was the wind speed considered for simulation purposes. With the above grid size, the computational time for crossing the convergence criteria of 10^{-8} was 8 h. 12 cores of the processor with 128 GB RAM was enough for the current simulation. From Figure 6, it can be observed that the outlet temperature deviation with the use of different turbulence models was much less. The flow occurred with a conduit having no interaction with the atmosphere; hence, flow prediction was not a prime task.

Numerical methods make use of the continuity equation (Equation (10)), momentum equation (Equation (11)), and energy equations (Equations (12) and (13)) simultaneously to provide heat interaction. For this purpose, commercial ANSYS CFX software was used in the study.

$$\frac{\partial \rho}{\partial t} + \nabla(\rho . \vec{v}) = S_m \tag{10}$$

$$\frac{\partial \vec{v}}{\partial t} + \nabla(\rho . \vec{v} . \vec{v}) = -\Delta p + \Delta \bar{\bar{\tau}} + \rho . \vec{g} + \vec{f} \tag{11}$$

Conjugate heat transfer,

$$\frac{\partial(\rho h)}{\partial t} + \nabla.(\rho U_s h) = \nabla.(\lambda \nabla T) + S_E \quad (12)$$

where h, ρ and λ are enthalpy, density, and thermal conductivity of the solid, respectively. S_E is the optional volumetric heat source.

Thermal energy equation,

$$\frac{\partial(\rho h)}{\partial t} + \nabla.(\rho U h) = \nabla.(\lambda \nabla T) + \tau : \nabla U + S_E \quad (13)$$

where $\tau : \nabla$ is always positive and is called viscous dissipation.

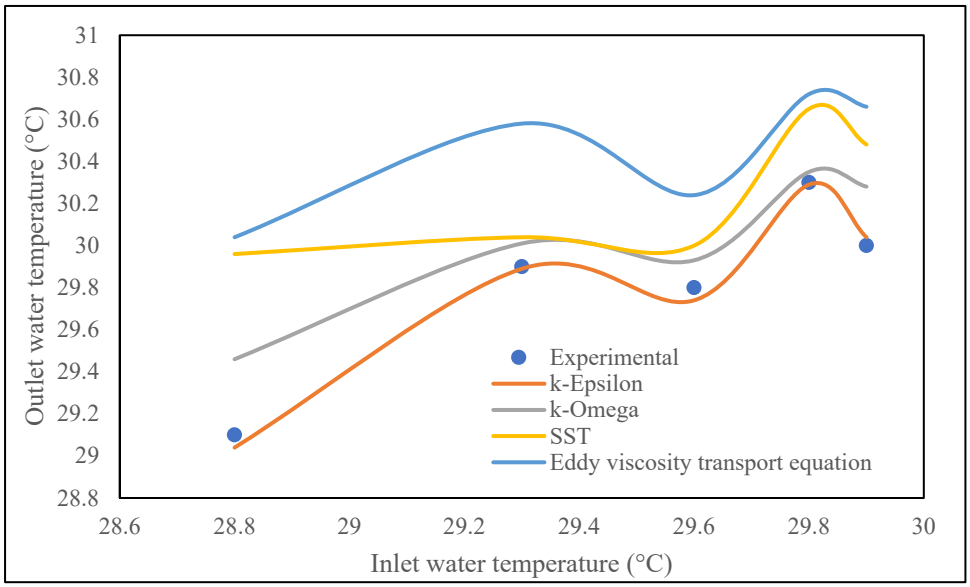

Figure 6. Validation of various models.

3. Results and Discussion

3.1. Experimental Results

Table 1 shows the variation in the outlet temperature of the water and thermal efficiency with different values of heat input. As clearly observed from Table 1, the thermal efficiency increases with the increase in heat input, which was clear to be an obvious phenomenon. Later parts of the manuscript will clearly justify the reason for the aforementioned statement. Tables 2–4 show the heat lost from various components and surfaces of the PV cell. Table 5 shows heat transfer because of convection and radiation from the bottom surface of the PV cell. Tables 6–8 show the heat lost from the pipe surface. Uncertainty (unpredictable) in heat transfer is also being tabulated. Figure 7 shows the irradiation measured using the digital solar meter for one day with bright sunlight.

Table 1. Variation of thermal efficiency with heat input.

Q_{input} (W)	T_{atm} (°C)	$T_{water,\ in}$ (°C)	$T_{water,\ out}$ (°C)	$\eta_{thermal}$
230.04	35.1	31.8	32.5	15.92
258.61	40.1	32.5	33.6	38.18
209.94	39.9	32.9	33.9	44.52
257.83	37.2	32.4	33.7	53.17
146.40	40.1	32.5	33.1	57.46
110.33	39.5	32.8	33.2	49.85
68.16	37.6	33.1	33.3	52.77
23.64	38.9	33.3	33.35	42.89

Table 2. Heat transfer through convection from a different cross section of PV cell.

$Q_{net\ input}$ (W)	Q_{glass} (W)	$Q_{adhesive}$ (W)	$Q_{pv\ cell}$ (W)	Q_{solder} (W)	$Q_{substrate}$ (W)	$Q_{total\ convection}$ (W)
197.16	3.78	0.13	0.15	0.13	2.57	6.75
208.54	2.73	0.09	0.11	0.09	1.85	4.87
167.44	1.98	0.07	0.08	0.07	1.33	3.52
212.21	2.05	0.07	0.08	0.07	1.38	3.65
118.44	1.13	0.04	0.04	0.04	0.73	1.98
90.86	0.87	0.03	0.03	0.03	0.55	1.51
59.95	1.02	0.03	0.04	0.03	0.66	1.79
21.06	0.40	0.01	0.02	0.01	0.23	0.66

Table 3. Heat transfer through radiation from a different cross section of PV cell.

$Q_{net\ input}$ (W)	Q_{glass} (W)	$Q_{adhesive}$ (W)	$Q_{pv\ cell}$ (W)	Q_{solder} (W)	$Q_{substrate}$ (W)	$Q_{total\ radiation}$ (W)
197.16	1.04531	0.00735	0.00881	0.00231	0.60657	1.67
208.54	0.76988	0.00541	0.00648	0.00170	0.44347	1.23
167.44	0.54640	0.00384	0.00460	0.00121	0.31155	0.87
212.21	0.55241	0.00388	0.00465	0.00122	0.31537	0.88
118.44	0.30449	0.00214	0.00255	0.00067	0.16872	0.48
90.86	0.23100	0.00162	0.00193	0.00051	0.12540	0.36
59.95	0.26901	0.00189	0.00225	0.00059	0.14804	0.42
21.06	0.10377	0.00072	0.00086	0.00022	0.05036	0.16

Table 4. Total heat transfer due to convection and radiation from a cross section of PV cell.

$Q_{net\ input}$ (W)	$Q_{convection}$ (W)	$Q_{radiation}$ (W)	$Q_{total,\ cross\ section}$ (W)
197.16	6.75	1.67	8.42
208.54	4.87	1.23	6.1
167.44	3.52	0.87	4.39
212.21	3.65	0.88	4.53
118.44	1.98	0.48	2.46
90.86	1.51	0.36	1.87
59.95	1.79	0.42	2.21
21.06	0.66	0.16	0.82

Table 5. Heat transfer due to convection and radiation from the back surface of the PV panel.

$Q_{net\ input}$ (W)	$Q_{conduction}$ (W)	$Q_{radiation}$ (W)	$Q_{total,\ PV\ cell,\ the\ back\ surface}$ (W)
197.16	4.82	2.83	7.65
208.54	3.44	2.06	5.49
167.44	2.45	1.43	3.88
212.21	2.54	1.45	3.99
118.44	1.32	0.76	2.08
90.86	0.98	0.55	1.53
59.95	1.18	0.66	1.84
21.06	0.35	0.20	0.55

Table 6. Heat transfer due to convection from pipe surface to atmosphere.

$Q_{net\ input}$ (W)	Q_I (W)	Q_{II} (W)	Q_{III} (W)	$Q_{total,\ convection}$ (W)
197.16	2.98	65.51	33.35	101.83
208.54	2.12	46.74	23.79	72.65
167.44	1.51	33.28	16.94	51.74
212.21	1.57	34.54	17.58	53.69
118.44	0.82	17.95	9.14	27.91
90.86	0.60	13.26	6.75	20.62
59.95	0.73	16.08	8.18	24.99
21.06	0.22	4.82	2.45	7.49

Table 7. Heat transfer due to radiation from pipe surface to atmosphere.

$Q_{net\ input}$ (W)	Q_I (W)	Q_{II} (W)	Q_{III} (W)	$Q_{total,\ radiation}$ (W)
197.16	0.13	1.09	0.61	1.84
208.54	0.10	0.80	0.45	1.34
167.44	0.07	0.55	0.31	0.93
212.21	0.07	0.56	0.31	0.95
118.44	0.04	0.29	0.16	0.49
90.86	0.03	0.21	0.12	0.36
59.95	0.03	0.26	0.14	0.43
21.06	0.01	0.08	0.04	0.13

Table 8. Total heat transfer from the surface of the pipe.

$Q_{net\ input}$ (W)	$Q_{convection}$ (W)	$Q_{radiation}$ (W)	$Q_{pipe,\ total}$ (W)
197.16	101.83	1.84	103.67
208.54	72.65	1.34	73.99
167.44	51.74	0.93	52.67
212.21	53.69	0.95	54.63
118.44	27.91	0.49	28.40
90.86	20.62	0.36	20.98
59.95	24.99	0.43	25.42
21.06	7.49	0.13	7.62

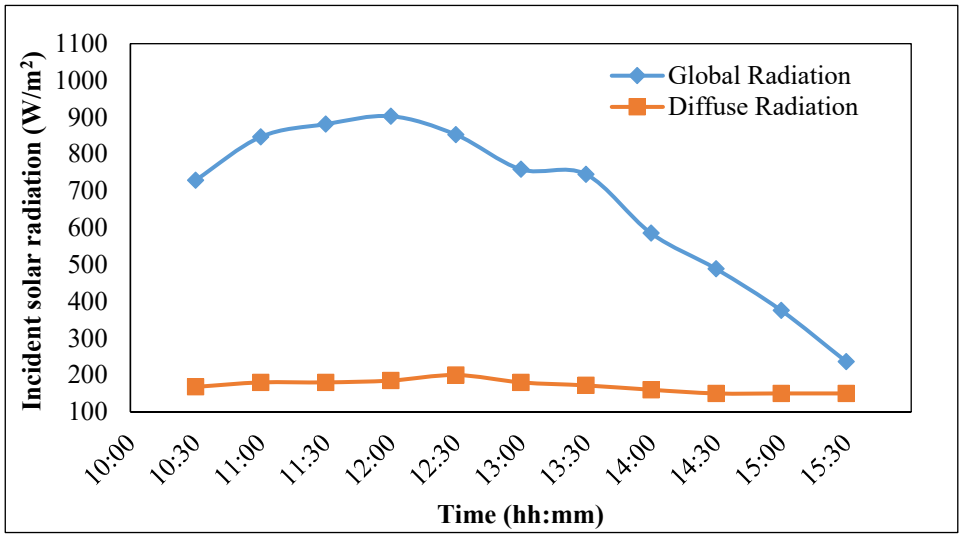

Figure 7. Variation of incident solar radiation during day time.

For different heat input, the heat transfer because of convection takes place from different cross sections of the PV cell. It can be observed that the majority of the heat transfer because of convection took place through glass and substrate. Similar patterns in

heat transfer because of radiation was observed. Still, heat transfer because of radiation was comparatively lower than heat transfer because of convection. The heat transfer from the back surface because of radiation was approximately 50% as that of heat transfer because of convection. The heat transfer from the pipe surface to the atmosphere because of convection took place mostly from surface II and then from surface I. Radiation heat transfer from the pipe surface was very low. Thus, the majority of heat transfer from the pipe surface was also because of convection. Table 9 shows the heat gained by water for different heat input calculated using Equation (12), while Table 10 shows the heat balance with uncertain heat loss magnitude. It was observed that of the total heat input, large amounts of heat were carried away by the water and pipe surface. Some amount of heat transfer takes place through the cross section and back surface of the PV cell. Thus, the heat input is balanced by the total heat lost after considering a few amounts in uncertain heat loss. As seen in Table 10, the uncertain magnitude of heat loss is below 6% of total heat input. Hence, the heat balance can be successfully concluded.

Table 9. Heat gained by water for different heat input.

$Q_{net\ input}$ (W)	$Q_{gained\ by\ water}$ (W)
197.16	73.15
208.54	114.95
167.44	104.5
212.21	135.85
118.44	62.7
90.86	41.8
59.95	20.9
21.06	5.225

Table 10. Uncertain heat lost for different heat input.

$Q_{net\ input}$ (W)	$Q_{total,\ cross\ section,\ PVcell}$ (W)	$Q_{total,\ PV\ cell,\ the\ back\ surface}$ (W)	$Q_{pipe,\ total}$	$Q_{gained\ by\ water}$ (W)	$Q_{total,\ lost}$ (W)	$Q_{uncertain}$ (W)
197.16	8.42	7.65	103.67	73.15	192.90	4.26
208.54	6.1	5.49	73.99	114.95	200.53	8.00
167.44	4.39	3.88	52.67	104.5	165.44	2.00
212.21	4.53	3.99	54.63	135.85	199.00	13.21
118.44	2.46	2.08	28.40	62.7	95.64	22.80
90.86	1.87	1.53	20.98	41.8	66.18	24.68
59.95	2.21	1.84	25.42	20.9	50.38	9.56
21.06	0.82	0.55	7.62	5.225	14.21	6.84

3.2. Numerical Results and Discussion

As seen in Figure 8, the trend line representing the points carries a slope of 1, which well-justifies the validation of the computation model and solver. The simulations are carried out at various heat inputs under different ambient conditions and different mass flow rates. For validation, simulations were carried out at two values of mass flow rate (0.025 kg/s and 0.05 kg/s). The different ambient conditions for which the simulations were carried out are shown in Table 11.

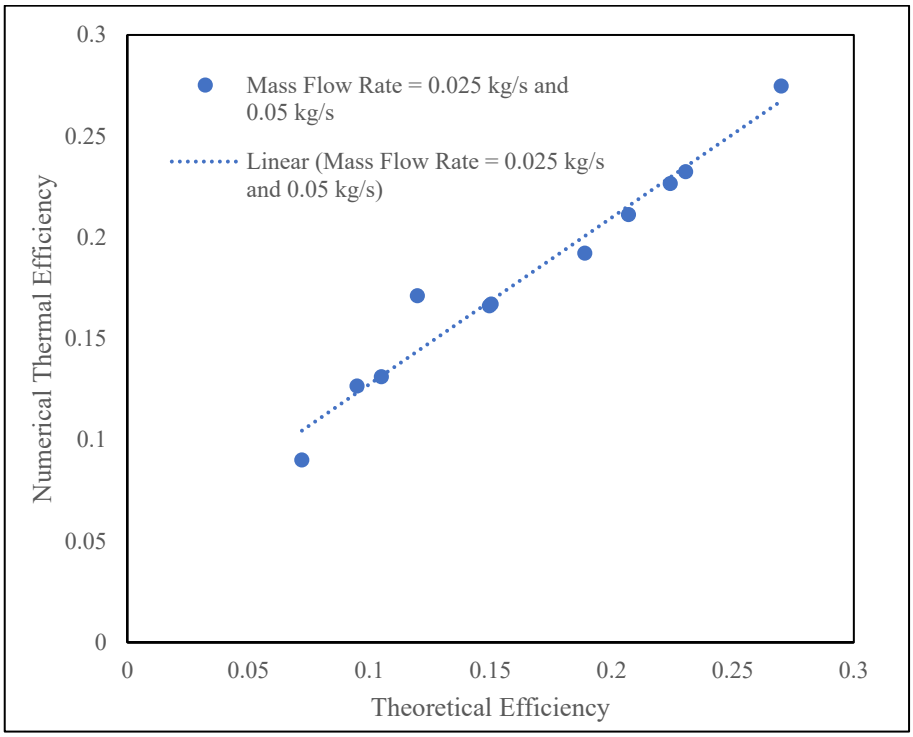

Figure 8. Theoretical versus numerical efficiency.

Table 11. Different ambient conditions considered for validation.

Net Heat Input (W/m^2)	Theoretical		Numerical Water Temperature Outlet in °C	Theoretical Thermal Efficiency	Numerical Thermal Efficiency
	Inlet Water Temperature in °C	Outlet Water Temperature in °C			
461.27	32.9	33.9	33.89	0.226547	0.224281
584.59	32.4	33.7	33.69	0.232385	0.230597
326.28	32.5	33.1	33.09	0.192167	0.188965
250.30	32.8	33.2	33.16	0.167	0.1503
165.14	33.1	33.3	33.25	0.12656	0.09492
58.00	33.3	33.35	33.34	0.090079	0.072063
478.09	28.8	29.1	29.04	0.131147	0.104918
503.01	28.8	29.2	29.16	0.166199	0.149579
494.78	29.8	30.3	30.29	0.211205	0.206981
456.55	29.3	29.9	29.89	0.274668	0.27009
244.25	29.6	29.8	29.74	0.171135	0.119794

In order to get a semi-empirical relation representing thermal efficiency in terms of *Re*, graphs for thermal efficiency versus inlet *Re* were plotted (Figure 9). This graph gives a better understanding of the variation in thermal efficiency due to inlet *Re* because of the variation in velocity of water at inlet. The graph also proved to be vital in validating the empirical relation with previous research [5,10,13].

For the instances where hour by hour (or other short time based) performance calculation for the system was required, it may be necessary to start with daily data of global and diffuse radiation. Radiation data are the best source of information for estimating average solar radiation. The effect of the atmosphere in scattering and absorbing radiation was variable with time as atmospheric condition. Sometimes global radiation values are in the middle range between cloudless days and completely cloudy days, such as heavy clouds and continuous light clouds. Figure 7 shows the hourly relative solar radiation intensity data of total and diffuse radiation for clear skies, measured with a thermopile pyrometer. It can be seen from the graph that global radiation starts increasing from the morning and

reaches the maximum point at noon hours and again starts to decline thereafter, whereas there was no significant variation in diffuse radiation. Average daily global radiation of 776 W/m^2 was observed, whereas the average daily diffuse radiation was 163 W/m^2.

As observed in Figure 9, the thermal efficiency of solar PV cells increases up to a particular limit and then remains constant. This is in accordance, considering all the irreversibilities and attending the second law efficiency. So, the thermal efficiency can be increased by varying the velocity at the inlet, density of the fluid, and characteristic length at the entry. The present work proposes a semi-empirical relation between the thermal efficiency and Reynolds number (Equation (14)), using regression analysis.

$$\eta_{Thermal} = 0.002 \times Re^{0.89} = f(Re) \quad (14)$$

Figure 10 shows the variation in electrical efficiency versus the ratio of heat carried away by water to heat input. From Figure 10, it was viable that the electrical efficiency varies significantly with the cooling of PV cells. When over 40% of the heat input was carried away by water, maximum electrical efficiency was achieved. The maximum electrical efficiency of the cooling cell under normal conditions was around 15% to 18%. This efficiency improved up to 20% with cooling. Thus, cooling of PV cells proved to be beneficial.

The decrease in efficiency with temperature was observed in the experimental setup as observed in the existing literature [2,3,25,27]. Cooling of the panel improves efficiency and the electrical output as seen in earlier findings [8,13,15,19,27]. A 9% to 20% improvement in thermal efficiency was also observed in our study, similar to Bahaidarah et al. [19] and Irwan et al. [19]. Transformation efficiency improvement by 4% to 5% was also observed, as discovered by Teo et al. [32]. Similar results were achieved through the numerical model, making it a reliable numerical model.

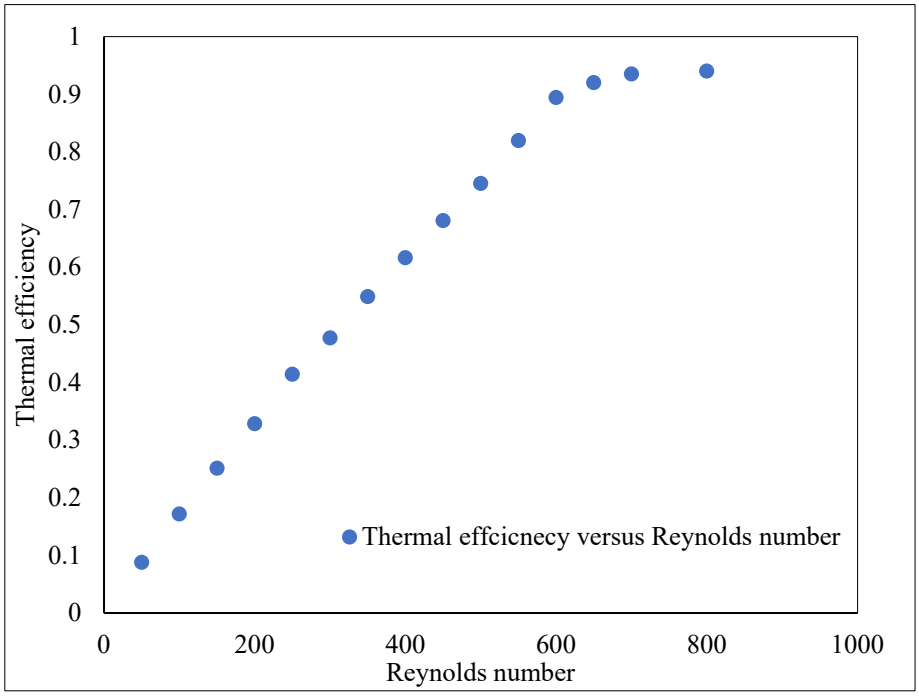

Figure 9. Graphical representation of thermal efficiency versus Reynolds number at inlet.

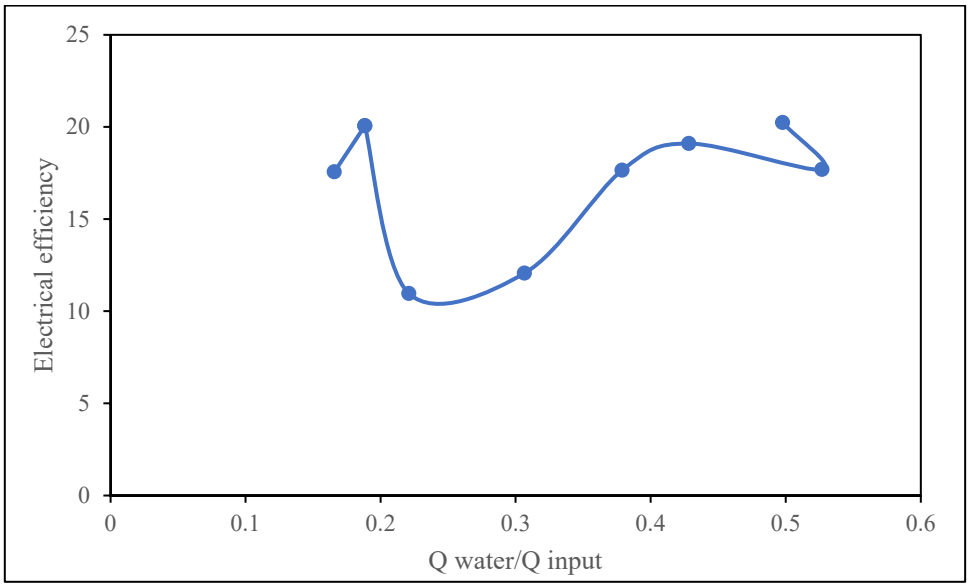

Figure 10. Electrical efficiency of PV cell.

4. Conclusions

The present work shows the validation of computational domain results with the experimental one for the PV system. It was seen that incident solar radiation, collector geometry, and cooling fluid and its configuration had a crucial role in solar-based power generation. The heat balance estimation was performed using the computational domain and our work concluded that uncertain heat loss was very low and validated the heat balance. The convective and radiative heat transfer through the PV cell and pipe surface were evaluated to estimate heat lost for different heat input. It was concluded that there is an optimum power input corresponding to $Re = 700$, which was required for cooling the PV cell. Beyond this value of power input, the cooling of the PV cell was impractical. The empirical relation between the thermal efficiency and Re ($\eta_{Thermal} = 0.002 \times Re^{0.89} = f(Re)$) evaluates the optimum power required for cooling to attain maximum efficiency. It was concluded that maximum electrical efficiency up to 20% can be achieved by the cooling of PV cells using water flowing under the panel when 40% of heat input was carried away by cooling water. Future research can validate the model for cooling fluids other than water.

Author Contributions: Conceptualization, E.A., M.N.A. and E.A.B.; Formal analysis, E.A., M.N.A. and E.A.B.; Funding acquisition, W.A.F.W.O.; Methodology, E.A., M.N.A. and E.A.B.; Project administration, W.A.F.W.O., E.A.B. and S.S.N.A.; Supervision, M.N.A. and E.A.B.; Writing—original draft, E.A.; Writing—review and editing, E.A., W.A.F.W.O. and S.S.N.A. All authors have read and agreed to the published version of the manuscript.

Funding: This study was funded by Research Creativity and Management Office, Universiti Sains Malaysia. The authors would like to acknowledge the grant RUTop-Down 1001/PAERO/870052.

Institutional Review Board Statement: Not Applicable.

Informed Consent Statement: Not Applicable.

Data Availability Statement: Not Applicable.

Conflicts of Interest: The authors declare no conflict of interest.

Abbreviations

Abbreviation	**Nomenclature**
PV	Photovoltaic
Re	Reynold number
V-I	Voltage-Current
Q	Heat transfer
T	Temperature
L	Thickness
K	Thermal Conductivity
A	Area
h	Convective heat transfer coefficient
m′	Mass flow rate
Cp	Specific heat at constant pressure
Subscript	**Nomenclature**
j	Refer to any quantity's outer surface
i	Refer to any quantity's inner surface
ij	Refer to any quantity's inner to outer surface
mat	Refer to material
s	Refer to surface
c,conv	Refer to any quantity in convection
rad	Refer to any quantity in radiation
a	Refer to ambient
6	Refer to surface 6 in Figure 2
Greek Notations	**Nomenclature**
ε	Emissivity
σ	Stefan Boltzmann constant
η	Efficiency

Appendix A

Turbulence Model

A: K-εmodel

$\mu_{eff} = \mu_t + \mu$

$\mu_t = \frac{C\,\rho\,K^2}{\in}$

K—Equation

$\frac{\partial\,(\rho K)}{\partial t} + \frac{\partial\,(\rho U_j K)}{\partial x_j} = \frac{\partial}{\partial x_j}\left\{\left[\,\mu + \frac{\mu_t}{\sigma_k}\right]\frac{\partial K}{\partial x_j}\right\} + P_k - \rho\varepsilon + P_{kb}$

$P_{kb} - Bouyant\ term = \mu_t\left[\frac{\partial U_j}{\partial x_j} + \frac{\partial U_j}{\partial x_j}\right] - \frac{2}{3}\frac{\partial U}{\partial x}\left[\,3\mu_t\frac{\partial U_k}{\partial x_k} + \rho K\right]$

ε—Equation

$\frac{\partial\,(\rho\varepsilon)}{\partial t} + \frac{\partial\,(\rho U_j \varepsilon)}{\partial x_j} = \frac{\partial}{\partial x_j}\left\{\left[\,\mu + \frac{\mu_t}{\sigma_\varepsilon}\right]\frac{\partial \varepsilon}{\partial x_j}\right\} + \frac{\varepsilon}{K}[C_{\varepsilon 1}P_k - C_{\varepsilon 2}\,P\varepsilon + C_{\varepsilon 1}P_{\varepsilon b}]$

B: Shear Stress Transport model

$\vartheta_t = \frac{a_1\,K}{\max(a_1,\,\omega, SF_2)}$

S—Invariant strain rate.

Takes combination effect of K-ε and K-ω

Behaves as K-ω in near-wall region and K- ε in the far wall region

$\frac{\partial\,(\rho K)}{\partial t} + \frac{\partial\,(\rho U_j K)}{\partial x_j} = \frac{\partial}{\partial x_j}\left\{[\,\mu + \sigma_k \mu_t]\frac{\partial K}{\partial x_j}\right\} + P_k - \beta\rho K\omega$

Does not considers buoyant force

Turbulence production term is modified

$\frac{\partial\,(\rho\omega)}{\partial t} + \frac{\partial\,(\rho U_j \omega)}{\partial x_j} = \frac{\partial}{\partial x_j}\left\{\left[\,\mu + \frac{\mu_t}{\sigma_\omega}\right]\frac{\partial \omega}{\partial x_j}\right\} + 2(1 - F_t)\rho\,\frac{1}{\rho_{\omega 2}}\frac{\partial K}{\partial x_j}\frac{\partial \omega}{\partial x_j} + \alpha_3\frac{\omega}{K}P_k - \beta\omega\rho^2$

F_t—Blend factor which switches in near wall and the far wall region

References

1. Jacak, J.E.; Jacak, W.A. Routes for Metallization of Perovskite Solar Cells. *Materials* **2022**, *15*, 2254. [CrossRef] [PubMed]
2. Sharaf, M.; Yousef, M.S.; Huzayyin, A.S. Review of cooling techniques used to enhance the efficiency of photovoltaic power systems. *Environ. Sci. Pollut. Res.* **2022**, *29*, 26131–26159. [CrossRef] [PubMed]
3. Verma, S.; Mohapatra, S.; Chowdhury, S.; Dwivedi, G. Cooling techniques of the PV module: A review. *Mater. Today Proc.* **2021**, *38*, 253–258. [CrossRef]
4. Zhao, B.; Hu, M.; Ao, X.; Xuan, Q.; Pei, G. Spectrally selective approaches for passive cooling of solar cells: A review. *Appl. Energy* **2020**, *262*, 114548. [CrossRef]
5. Ghadikolaei, S.S.C. Solar photovoltaic cells performance improvement by cooling technology: An overall review. *Int. J. Hydrog. Energy* **2021**, *46*, 10939–10972. [CrossRef]
6. Akbarzadeh, A.; Wadowski, T. Heat pipe-based cooling systems for photovoltaic cells under concentrated solar radiation. *Appl. Therm. Eng.* **1996**, *16*, 81–87. [CrossRef]
7. Anderson, W.G.; Dussinger, P.M.; Sarraf, D.B.; Tamanna, S. Heat pipe cooling of concentrating photovoltaic cells. In Proceedings of the 2008 33rd IEEE Photovoltaic Specialists Conference, San Diego, CA, USA, 11–16 May 2008; IEEE: Washington, DC, USA, 2008; pp. 1–6.
8. Abdolzadeh, M.; Ameri, M. Improving the effectiveness of a photovoltaic water pumping system by spraying water over the front of photovoltaic cells. *Renew. Energy* **2009**, *34*, 91–96. [CrossRef]
9. Kordzadeh, A. The effects of nominal power of array and system head on the operation of photovoltaic water pumping set with array surface covered by a film of water. *Renew. Energy* **2010**, *35*, 1098–1102. [CrossRef]
10. Alami, A.H. Effects of evaporative cooling on efficiency of photovoltaic modules. *Energy Convers. Manag.* **2014**, *77*, 668–679. [CrossRef]
11. Brinkworth, B.J.; Cross, B.M.; Marshall, R.H.; Yang, H. Thermal regulation of photovoltaic cladding. *Sol. Energy* **1997**, *61*, 169–178. [CrossRef]
12. Bione, J.; Vilela, O.C.; Fraidenraich, N. Comparison of the performance of PV water pumping systems driven by fixed, tracking and V-trough generators. *Sol. Energy* **2004**, *76*, 703–711. [CrossRef]
13. Bahaidarah, H.; Subhan, A.; Gandhidasan, P.; Rehman, S. Performance evaluation of a PV (photovoltaic) module by back surface water cooling for hot climatic conditions. *Energy* **2013**, *59*, 445–453. [CrossRef]
14. Chen, Q.; Yang, K.; Wang, M.; Pan, N.; Guo, Z.-Y. A new approach to analysis and optimization of evaporative cooling system I: Theory. *Energy* **2010**, *35*, 2448–2454. [CrossRef]
15. Du, B.; Hu, E.; Kolhe, M. Performance analysis of water cooled concentrated photovoltaic (CPV) system. *Renew. Sustain. Energy Rev.* **2012**, *16*, 6732–6736. [CrossRef]
16. Farahat, M.A. Improvement the thermal electric performance of a photovoltaic cells by cooling and concentration techniques. In Proceedings of the 39th International Universities Power Engineering Conference, Bristol, UK, 6–8 September 2004; IEEE: Washington, DC, USA, 2004; Volume 2, pp. 623–628.
17. Hughes, B.R.; Cherisa, N.P.S.; Beg, O. Computational study of improving the efficiency of photovoltaic panels in the UAE. *World Acad. Sci. Eng. Technol.* **2011**, *73*, 278–287.
18. Hasan, H.A.; Sopian, K.; Ameen, K.A. Numerical investigation of Microjet impingement of water for cooling photovoltaic solar cell. *J. Adv. Res. Fluid Mech. Therm. Sci.* **2018**, *51*, 71–79.
19. Irwan, Y.M.; Leow, W.Z.; Irwanto, M.; Amelia, A.R.; Gomesh, N.; Safwati, I. Indoor test performance of pv panel through water cooling method. *Energy Procedia* **2015**, *79*, 604–611. [CrossRef]
20. Kerzmann, T.; Schaefer, L. System simulation of a linear concentrating photovoltaic system with an active cooling system. *Renew. Energy* **2012**, *41*, 254–261. [CrossRef]
21. Chong, K.-K.; Tan, W.-C. Study of automotive radiator cooling system for dense-array concentration photovoltaic system. *Sol. Energy* **2012**, *86*, 2632–2643. [CrossRef]
22. Fujii, M.; Yanagihara, H.; Mitsumoto, S.; Kikugawa, S.; Tokoro, T.; Fukuma, M. Improvement of conversion efficiency through water-cooled equipment in photovoltaic system. *J. Int. Counc. Electr. Eng.* **2013**, *3*, 97–101. [CrossRef]
23. Nižetić, S.; Čoko, D.; Yadav, A.; Grubišić-Čabo, F. Water spray cooling technique applied on a photovoltaic panel: The performance response. *Energy Convers. Manag.* **2016**, *108*, 287–296. [CrossRef]
24. Omubo-Pepple, V.B.; Israel-Cookey, C.; Alaminokuma, G.I. Effects of temperature, solar flux and relative humidity on the efficient conversion of solar energy to electricity. *Eur. J. Sci. Res.* **2009**, *35*, 173–180.
25. Park, K.E.; Kang, G.H.; Kim, H.I.; Yu, G.J.; Kim, J.T. Analysis of thermal and electrical performance of semi-transparent photovoltaic (PV) module. *Energy* **2010**, *35*, 2681–2687. [CrossRef]
26. Royne, A.; Dey, C.J.; Mills, D.R. Cooling of photovoltaic cells under concentrated illumination: A critical review. *Sol. Energy Mater. Sol. Cells* **2005**, *86*, 451–483. [CrossRef]
27. Krauter, S. Increased electrical yield via water flow over the front of photovoltaic panels. *Sol. Energy Mater. Sol. Cells* **2004**, *82*, 131–137. [CrossRef]
28. Schnitzer, H.; Brunner, C.; Gwehenberger, G. Minimizing greenhouse gas emissions through the application of solar thermal energy in industrial processes. *J. Clean. Prod.* **2007**, *15*, 1271–1286. [CrossRef]

29. Skoplaki, E.; Palyvos, J.A. On the temperature dependence of photovoltaic module electrical performance: A review of efficiency/power correlations. *Sol. Energy* **2009**, *83*, 614–624. [CrossRef]
30. Rehman, S.; El-Amin, I. Performance evaluation of an off-grid photovoltaic system in Saudi Arabia. *Energy* **2012**, *46*, 451–458. [CrossRef]
31. Salih, S.M.; Abd, O.I.; Abid, K.W. Performance enhancement of PV array based on water spraying technique. *Int. J. Sustain. Green Energy* **2015**, *4*, 8–13.
32. Teo, H.G.; Lee, P.S.; Hawlader, M.N.A. An active cooling system for photovoltaic modules. *Appl. Energy* **2012**, *90*, 309–315. [CrossRef]